# Noise analysis of an InAsSb single heterojunction photovoltaic detector for free-space optical communication (FOC) applications

P. K. MAURYA, P. CHAKRABARTI*
*Centre for Research in Microelectronics, Department of Electronics Engineering, Institute of Technology, Banaras Hindu University, Varanasi-221005, India*

The noise analysis of a long-wavelength infrared (LWIR) photodetector based on $InAs_{1-x}Sb_x$ has been reported. The noise equivalent power limited by thermal and shot noise current components has been estimated theoretically by considering a simplistic model of the photodetector. All the dominant dark current components e.g., diffusion, generation-recombination and tunneling (both band-to-band and trap-assisted) have been taken into consideration for computation of shot-noise. The noise equivalent power (NEP) has been estimated to be $3.35\times10^{-11}$ $WHz^{1/2}$ for an equivalent load resistance of 1 MΩ for operation at 77 K. The physics based model developed for photodetector characterization has been validated by reported experimental results.

(Received September 25, 2007; accepted October 31, 2007)

*Keywords:* InAsSb photodetector, Tunneling, Noise, free-space optical communication (FSO), noise equivalent power (NEP)

## 1. Introduction

InAsSb based long-wavelength infrared (LWIR) photodetectors operating in the 2-13 μm spectral range find application in free space optical communication. Free space optical communication represents one of the most promising approaches for addressing the emerging broadband access market. In recent years free space optical communication (FSO) has drawn considerable interest in commercial and military applications due to high available bandwidths, portability and high security of such systems. The other advantages of free space optical communication over optical fiber communication include quick link set up, rapid deployment time, license- and tariff-free bandwidth allocation, low power consumption etc. These systems are also compatible to a wide range of other communication system and are sufficiently flexible so as to be easily implemented using a variety of different architectures. Several researchers have already established that infrared region is best suited for free space optical communication [1]-[2]. In free space optical communication system the photodetector is the key component in the receiver unit. There are a number of atmospheric attenuation windows in the long-wavelength region which are suitable for establishing efficient free space optical link. Two such strategic wavelengths for application in free space optical system are 9.6 μm and 10.6 μm. Successful implementation of free space optical communication receiver at these wavelengths requires development of suitable photodetectors operating at these wavelengths. Both III-V and II-VI narrow bandgap semiconductor are potential candidates for development of such detectors. The energy bandgap of narrow-band II-VI and III-V alloy semiconductors can be tailored suitably by adjusting the mole fraction of the constituent elements so as to match with the desired wavelength of emission or absorption. The ternary alloys $Hg_{1-x}Cd_xTe$ (II-VI) and $InAs_{1-x}Sb_x$ (III-V) are principal materials used for fabrication of long wavelength infrared (LWIR) photodetectors. The advantages of $InAs_{1-x}Sb_x$ over $Hg_{1-x}Cd_xTe$ include higher electron and hole mobilities and high-quality and low-cost substrates. The performance of such devices is strongly influenced by several factors which are special to narrow bandgap semiconductors. The operation of such devices is highly restricted by the requirement of low temperature operation. The noise performance of the detectors based on narrow bandgap materials is also influenced by a large value of dark current at room temperature. A number of long-wavelength infrared photodetectors based on InAsSb have been proposed, fabricated and characterized by several workers in the past [3]-[9] for several non-telecommunication applications. However, a complete noise analysis of the photodetector for examining the potential of these devices for application in optical receivers has not been reported so far. In this paper we report a complete noise analysis of an InAsSb based long-wavelength infrared (LWIR) photodetector for theoretical characterization of the device as an optical to electrical converter in a free space optical communication receiver operating at 10.6 μm.

## 2. Noise analysis

The structure under consideration is a heavily doped n-type InSb layer, a lightly doped p-type (π-type) $InAs_{1-x}Sb_x$ active region, and a heavily doped InSb p-type cladding layer. The structure is supposed to be grown on lattice-matched GaAs substrate. Here $N^+$- InSb acts as a

buffer layer with 14.5% lattice-mismatch to GaAs. The absorption of optical radiation in the π-$InAs_{1-x}Sb_x$ region results in generation of electron and hole pairs in addition to existing thermally generated carriers. In order to study the noise properties in photodiode, we consider the generalized photodetection process shown in Fig.1 (a) in which the photodetector acts as a simple photon counter and the incoming signal is considered to be intensity modulated optical signal. Under the influence of electric field in the depletion region the photogenerated electron–hole pairs generated in this region and those diffused into it drift towards their opposite sides in p-n junction. The noise behavior of photodetector is determined by two basic contributions, namely shot noise and thermal noise. Shot noise is caused by the random fluctuation of current flowing through device. The absorption of optical radiation leads to random generation of electron-hole pairs which gives rise to quantum noise. This noise component is ultimately manifested in the form of shot noise. The mean square value of shot noise current in presence of optical signal can be written as

$$\left\langle i_s^2 \right\rangle = 2q\left(I_{photo} + I_{dark}\right)B \tag{1}$$

where B is the bandwidth, $I_{photo}$ and $I_{dark}$ are the d-c value of photocurrent and dark current respectively. The photodiode is further terminated to load resistance which sees the input impedance of the following amplifier stage. The simplified noise equivalent circuit of the photodetector is shown in Fig. 1(b). The signal and noise current (shot and thermal) are decided by random noise current. The device capacitance $C_j$ is essentially the junction capacitance of the detector and $R_j$, $R_s$, $R_L$ are the junction resistance, series resistance of the detector, load resistance respectively. In the analysis the series resistance $R_s$ is ignored for the purpose of noise calculation.

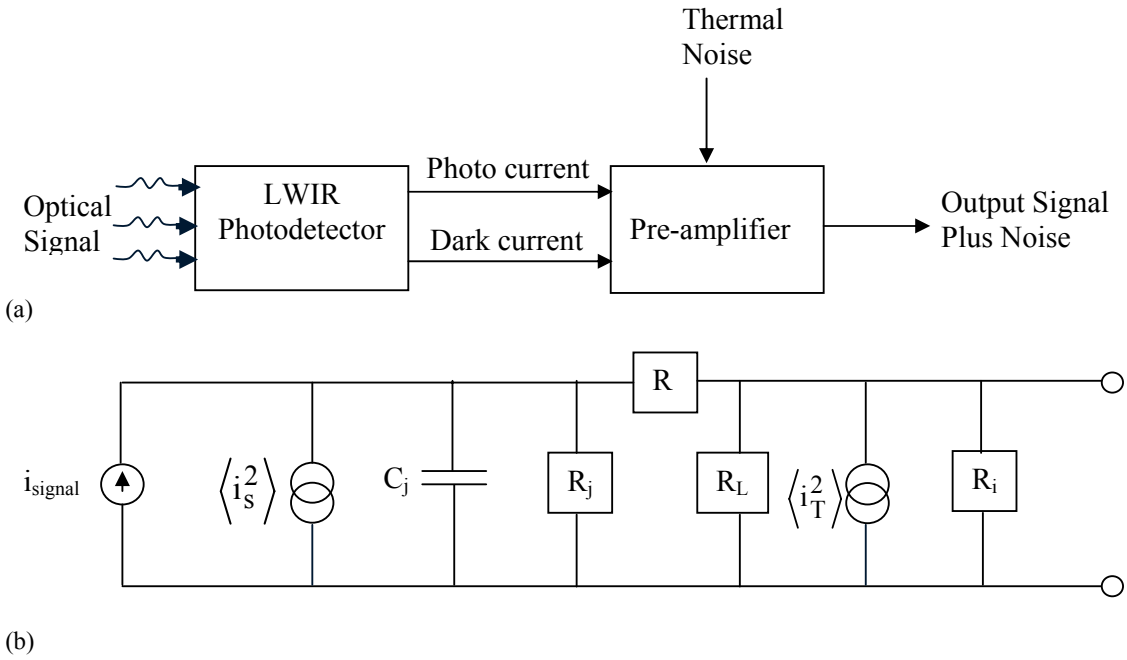


*Fig. 1. (a) Components of current in photodetector process (b) Equivalent circuit of the photodiode.*

### 2.1 Photocurrent

The incident optical power has been assumed to be intensity modulated in the form

$$P(t) = P_{opt}\left(1 + \mu\cos(2\pi ft)\right) \tag{2}$$

where $P_{opt}$ is the optical power at wavelength λ, $\mu$ is the index of modulation and $f$ is the frequency of the modulating signal.

The root-mean-square value of the signal can be obtained as

$$i_{signal} = \frac{1}{\sqrt{2}}\frac{q\eta\mu P_{opt}}{h\nu} \tag{3}$$

where η is the quantum efficiency and hν is the energy of the photons corresponding to radiation of wavelength λ . The average photocurrent due to the incident optical signal is given by

$$I_{photo} = \frac{q\eta P_{opt}}{h\nu} \tag{4}$$

The mean square value of the thermal noise current for the photodetector can be expressed as

$$\left\langle i_T^2 \right\rangle = \frac{4kT}{R_{eq}} B \qquad (5)$$

where k is Boltzmann's constant, T is the absolute temperature and $R_{eq}$ is the equivalent resistance given by

$$\frac{1}{R_{eq}} = \frac{1}{R_j} + \frac{1}{R_L} + \frac{1}{R_i} .$$

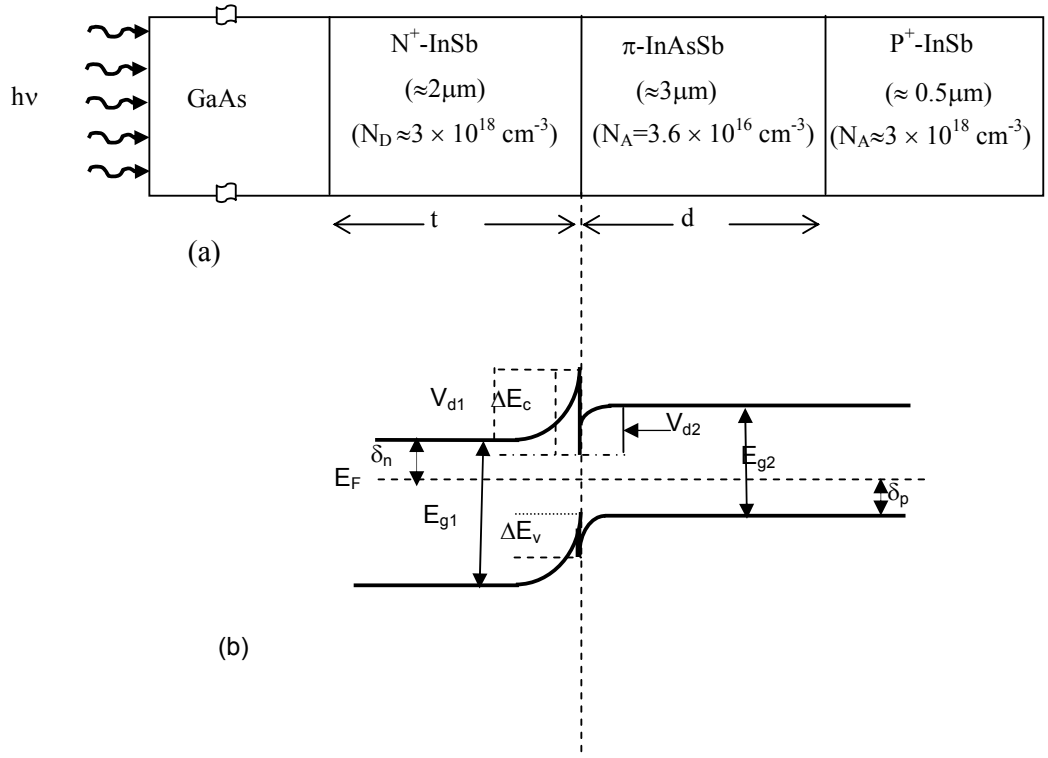


*Fig. 2. (a) Schematic diagram of the detector structure (b) energy band diagram.*

The signal to noise ratio at the input of the amplifier can be obtained as

$$\left(\frac{S}{N}\right)_{power} = \frac{i_{signal}^2 R_{eq}}{\left(\left\langle i_s^2 \right\rangle + \left\langle i_T^2 \right\rangle\right) R_{eq}} = \frac{\frac{1}{2}\left(\frac{q\eta\mu P_{opt}}{h\upsilon}\right)^2}{2q\left(I_{photo} + I_{dark}\right)B + \frac{4kT}{R_{eq}}B} \qquad (6)$$

$$\left(P_{opt}\right)_{\min} = \frac{2h\nu B}{\eta}\left(\frac{S}{N}\right)\left\{1 + \left[1 + \frac{I_{eq}}{qB\left(\frac{S}{N}\right)}\right]^{\frac{1}{2}}\right\} \qquad (7)$$

where $$I_{eq} = I_{dark} + \frac{2kT}{qR_{eq}}$$

In order to quantify detector noise, a good figure of merit to use is the Noise Equivalent Power (NEP). The noise-equivalent-power (NEP) of the photodetector is defined as the root-mean-square value of the input optical power needed to produce a signal power at the output that is equal to total noise power developed at the output (in the case input of the following amplifier stage) for unity bandwidth of the photodetector. For a large value of $I_{eq}$, the NEP can be approximated as

$$NEP = \sqrt{2}\left(\frac{h\upsilon}{\eta}\right)\left(\frac{I_{eq}}{q}\right)^{1/2} \qquad (8)$$

### 2.2 Dark current

The structure under consideration shown in Fig.2 along with the energy band diagram. The dark current density of the InAsSb photodetector has been modeled here by considering (i) the diffusion of the thermally generated carriers from the neutral regions, $J_{diff;}$ (ii) generation-recombination of carriers in the depletion region, $J_{gr}$ and (iii) tunneling of carriers through the barrier, $J_{tun}$. In order to generalize the analysis, we have however considered both trap assisted tunneling as well as band-to-band tunneling. The tunneling component of current density thus constitutes two components e.g., $J_{tat}$ arising from the trap assisted tunneling and $J_{btb}$ arising out

of band-to-band tunneling. The net current density can be written as

$$J_{dark} = J_{diff} + J_{gr} + J_{tat} + J_{btb} \quad (9)$$

### 2.2.1 Diffusion component

In order to model the diffusion component of current density in mid-infrared photodetectors it is necessary to estimate the effective lifetime of the extracted carriers. There are three mechanisms of carrier recombination in the device under consideration. These include (i) Svhockley-Read-Hall (SRH) process via lattice defect and impurity level within the forbidden gap (ii) radiative process arising out of direct band-to-band transition and (iii) non-radiative Auger recombination, a three-state transition process. Among these three processes, the first one (SRH) can be easily controlled by improving the fabrication procedure. The other two mechanisms are prevalent in photovoltaic detectors made of narrow bandgap (direct) semiconductors. Further, Auger process becomes more dominant as the temperature increases and becomes crucial at or near room temperature [10]. It is understood that Auger mechanism is most likely to impose the fundamental limit to the performance of photovoltaic detectors based on narrow bandgap materials like InSb and related materials operating at or near room temperature. In the present analysis an exhaustive model of this mechanism [11]-[13] has been used. There are at least ten different possible Auger transitions in narrow bandgap InSb like band structures. For sake of simplicity we have considered the three most dominant Auger mechanisms only, e.g. Auger 1 (A-1), Auger 7 (A-7) and Auger S (A-S). Out of the above three transitions Auger 1 and Auger 7 are observed at smallest threshold energies and are generally important in practice. The other component (i.e. Auger S which occurs through conduction band/heavy hole band/spin split-off band) is generally dominant in the materials in which the spin-orbit splitting energy $\Delta$ approaches the bandgap energy. For the structure under consideration the bandgap energy of $InAs_{1-x}Sb_x$ (~0.1 eV) is much less than the spin-orbit split-off energy (~0.4 eV) and therefore A-S transition has been neglected in the present analysis. The effective carrier lifetime due to Auger recombination can then be written as

$$\frac{1}{\tau_{AU}} = \frac{1}{\tau_{A-1}} + \frac{1}{\tau_{A-7}} \quad (10)$$

where $\tau_{AU}$ corresponds to the overall value of the mean lifetime of the carriers due to Auger recombination and the other suffixes indicate the components of $\tau$ for the corresponding Auger transitions [14].

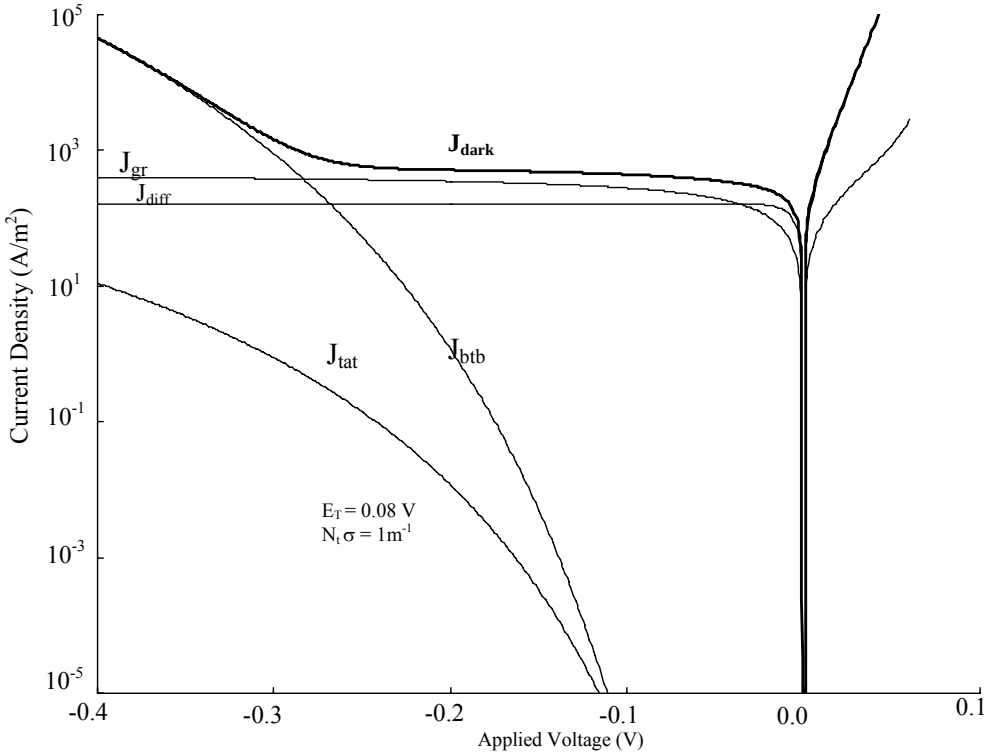


*Fig. 3. Variation of current density and its components with applied voltage.*

For direct bandgap semiconductors, the lifetime of carriers due to radiative and non-radiative Svhockley-Read-Hall recombination can be written as

$$\tau_{RAD} = \frac{1}{B_r\left(p_{no} + p_{p0}\right)} \tag{11}$$

$$\tau_{SRH} = \frac{1}{\sigma N_t v_{th}} \text{ and } v_{th} = \sqrt{\frac{3kT}{m_n^*}} \tag{12}$$

where $B_r$ is the radiative recombination coefficient of the material and $p_{no}$ and $p_{po}$ are the electron and hole concentrations in the region under thermal equilibrium, $N_t$ is the SRH trap density, $\sigma$ is the capture cross section and $v_{th}$ is the thermal velocity of the minority carriers in the active region.

The effective lifetime of the carriers in the semiconductor can be evaluated as

$$\frac{1}{\tau_{eff}} = \frac{1}{\tau_{AU}} + \frac{1}{\tau_{RAD}} + \frac{1}{\tau_{SRH}} \tag{13}$$

The diffusion component of current density for electrons and holes can be obtained as

$$J_{sn} = qn_{po}\frac{D_n}{L_n}\frac{\frac{L_nS_n}{D_n}\cosh\left(\frac{d-x_p}{L_n}\right)+\sinh\left(\frac{d-x_p}{L_n}\right)}{\frac{L_nS_n}{D_n}\sinh\left(\frac{d-x_p}{L_n}\right)+\cosh\left(\frac{d-x_p}{L_n}\right)}\exp\left[-\frac{qV_{d1}}{kT}\right] \tag{14}$$

$$J_{sp} = q\,p_{no}\frac{D_p}{L_p}\frac{\frac{L_pS_p}{D_p}\cosh\left(\frac{t-x_n}{L_p}\right)+\sinh\left(\frac{t-x_n}{L_p}\right)}{\frac{L_pS_p}{D_p}\sinh\left(\frac{t-x_n}{L_p}\right)+\cosh\left(\frac{t-x_n}{L_p}\right)}\exp\left[-\frac{q\left(V_d-\Delta E_c\right)}{kT}\right] \tag{15}$$

where $N_A$ and $N_D$ are the acceptor and donor concentrations in the $\pi$ and $N^+$ regions, respectively at equilibrium, $L_n$ and $L_p$ are the diffusion lengths for electrons and holes on the p and n side respectively, $D_n$ and $D_p$ are their respective diffusion coefficients, $S_n$ and $S_p$ are the surface recombination velocities for electrons and holes at the heterointerfaces. Here, $n_{po}$ and $p_{no}$ are the equilibrium minority carrier concentration on the $\pi$ and $N^+$- side of the heterointerfaces respectively, $x_p$ and $x_n$ are the widths of the depletion region on the respective sides, d is the thickness of active layer, t is the thickness of cladding layer, $V_{d1}$ is the barrier voltage at $N^+$- side and $V_d$ is the total barrier voltage.

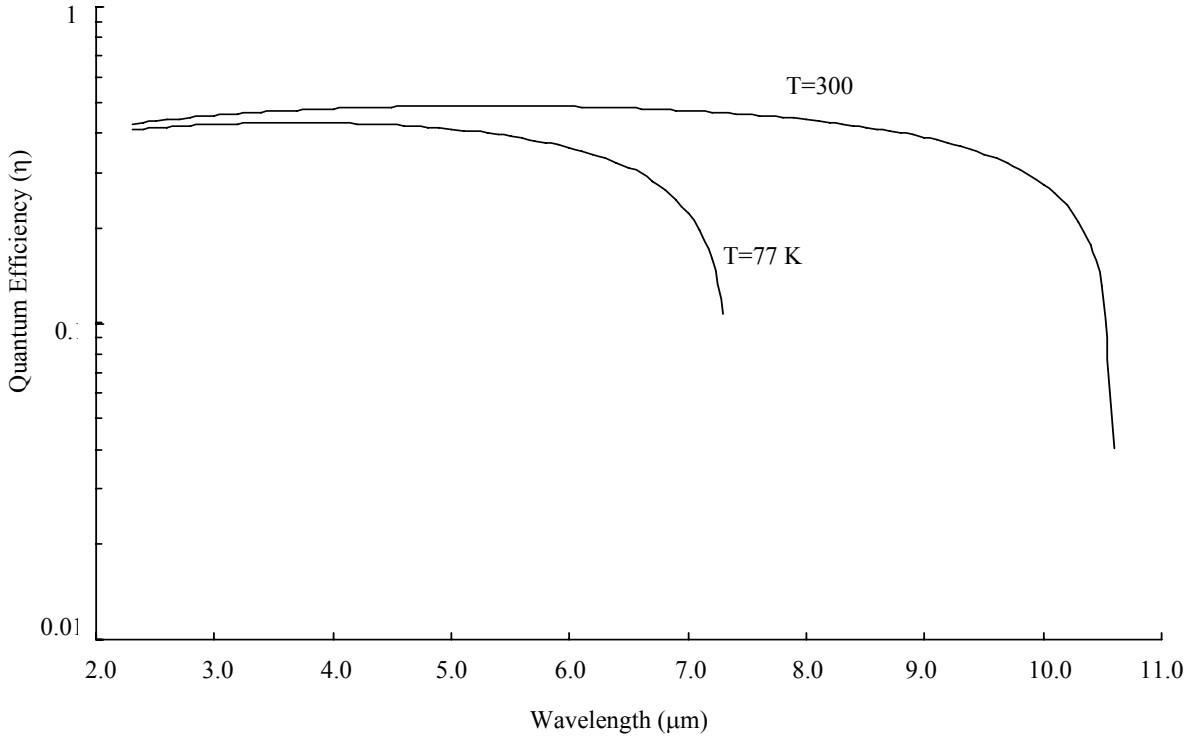


*Fig. 4. Variation of the quantum efficiency with operating wavelength at two different values of temperature (77 K and 300 K).*

The total diffusion current density for a applied voltage V can be obtain as

$$J_{diff} = \left(J_{sn} + J_{sp}\right)\left(\exp\left(\frac{qV}{kT}\right) - 1\right) \tag{16}$$

### 2.2.2 Generation-Recombination component

The carriers generated in the depletion region are generally separated out under the action of the existing electric field. These carriers contribute to the total current flowing through the detector. The transport of carriers across the heterojunction under consideration is strongly affected by the trap levels at the heterointerface inside the depletion region. The current density component arising from generation-recombination can be given as [15]

$$J_{gr} = \frac{qn_i W V}{(V_d - V)\,\tau_{SRH}}$$

$$\text{for } V < 0 \tag{17}$$

$$J_{gr} = \frac{2n_i W kT}{(V_d - V)\,\tau_{SRH}} \sinh\left(\frac{qV}{2kT}\right)$$

$$\text{for } V>0 \tag{18}$$

where $n_i$ is the intrinsic carrier concentration in π-InAsSb region, W is the total width of the depletion region.

### 2.2.3 Tunneling component

In the present heterojunction photodetector, the electrons and holes are separated on both sides of the heterointerface. The electrons and holes having energy below the barrier can cross the heterointerface by quantum mechanical tunneling process when the width of the barrier is sufficiently thin. As tunneling is a quantum mechanical process, one has to take help of quantum mechanics to model the tunneling current component. The components of dark current density arising from quantum mechanical tunneling can be obtained as [15]

$$J_{tat} = \frac{q^4 m_n^* E M^2 W N_T}{\hbar^3 (E_g - E_t)} \exp\left(-\frac{4\sqrt{2m_n^*}\,(E_g - E_t)^{3/2}}{3qE\hbar}\right) \tag{19}$$

where, $m_n^*$ is the electron effective mass, M is the Matrix element associated with trap potential, E is the electric field across the depletion region, $N_T$ is the trap density responsible for trap-assisted-tunneling and this trap density is different from the SRH trap density $N_t$. $E_T$ is the position of the trap energy level in the bandgap measured from the bottom of the conduction band.

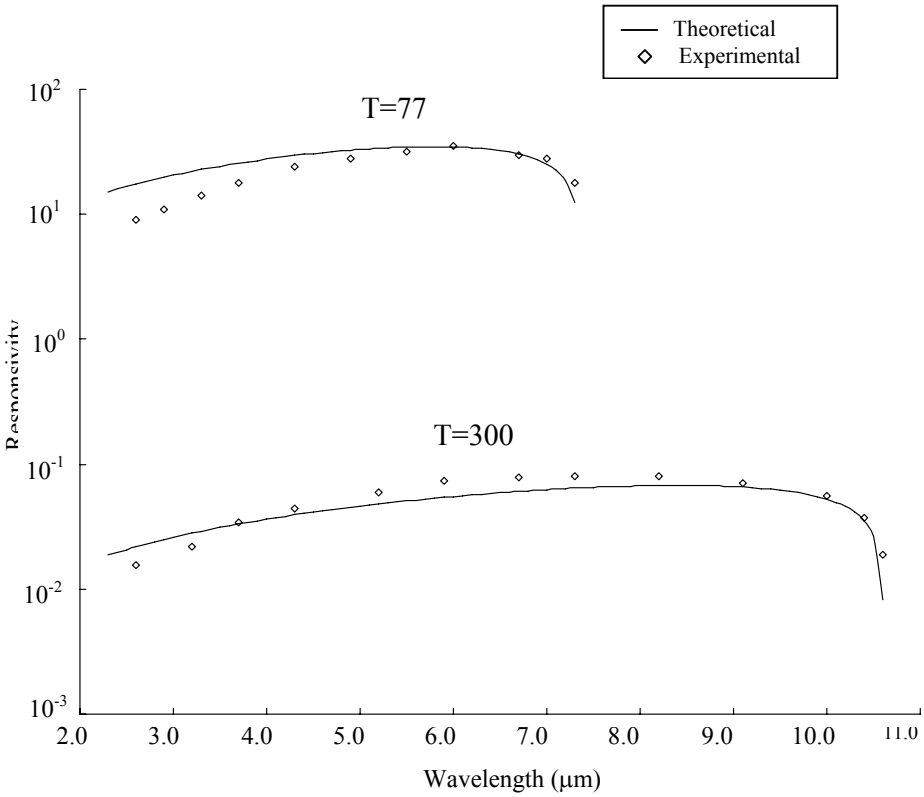


*Fig. 5. Variation of voltage responsivity with operating wavelength showing the theoretically predicted values and reported experimental data for 77 K and 300 K*

Band-to-band tunneling component of the dark current is given by [16]

$$J_{btb} = \frac{\sqrt{2m_n^*}\,q^3 EV}{4\pi^2\hbar^2 E_g^{1/2}} \exp\left(-\frac{4\sqrt{2m_n^*}\,E_g^{3/2}}{3qE\hbar}\right) \tag{20}$$

### 2.3 Quantum efficiency

The quantum efficiency (η) of the heterojunction photodetector under consideration has three components arising from the contribution of the three regions e.g., neutral n-region ($\eta_n$), neutral p-region ($\eta_p$) and the depletion region ($\eta_{dep}$). In the present analysis the radiation has been assumed to be incident from the receiver end made of GaAs substrate. The optical generation rate of electron and hole pairs, as a function of distance x from the surface in the $N^+$-InSb can be written as

$$G_n = \alpha_n(\lambda)(1-r_n)\left(\frac{P_{op}}{Ah\nu}\right)\exp(-\alpha_n(\lambda)x) \quad (21)$$

where $\alpha_n(\lambda)$ is the optical absorption coefficient of the $N^+$-InSb material which is a function of wavelength, $r_n$ is the Fresnel reflection coefficient at the entrance, $P_{op}$ is the incident optical power, ν is the frequency of radiation and A is the device area. The distance x is measured from the GaAs/$N^+$-InSb interface. The generation in the active p region can be written as

$$G_p = \alpha_p(\lambda)(1-r_n)\left(\frac{P_{op}}{Ah\nu}\right)\exp(-\alpha_n(\lambda)t)\exp(-\alpha_p(\lambda)x) \quad (22)$$

where $\alpha_p(\lambda)$ is the absorption coefficient of π-InAsSb region and t is the thickness of the $N^+$-InSb region.

The quantum efficiency due to the contribution of the photo-generated carriers in the depletion region can be obtained as

$$\eta_{dep}(\lambda) = (1-r_n)\left[\exp(-\alpha_n(t-x_n)) - \exp(-(\alpha_n t + \alpha_p x_p))\right] \quad (23)$$

The quantum efficiency components contributed by the neutral $N^+$-InSb and π-InAsSb regions can be obtained as

$$\eta_n(\lambda) = \frac{(1-r_n)\alpha_n L_p}{\alpha_n^2 L_p^2 - 1}\left[\frac{\alpha_n L_p + \gamma_p}{\gamma_p \sinh\left(\frac{t-x_n}{L_p}\right) + \cosh\left(\frac{t-x_n}{L_p}\right)} - \alpha_n L_p \exp\{-\alpha_n(t-x_n)\} - \frac{\exp\{-\alpha_n(t-x_n)\}\left[\gamma_p \cosh\left(\frac{t-x_n}{Lp}\right) + \sinh\left(\frac{t-x_n}{Lp}\right)\right]}{\gamma_p \sinh\left(\frac{t-x_n}{L_p}\right) + \cosh\left(\frac{t-x_n}{L_p}\right)}\right] \quad (24)$$

$$\eta_p(\lambda) = \frac{(1-r_n)\ \alpha_p L_n}{\alpha_p^2 L_n^2 - 1}\exp\{-(\alpha_n t + \alpha_p x_p)\} \times \left[\frac{(\gamma_n - \alpha_p L_n)\exp(-\alpha_p(d-x_p)) - \left[\gamma_n \cosh\left(\frac{d-x_p}{L_n}\right) + \sinh\left(\frac{d-x_p}{L_n}\right)\right]}{\gamma_n \sinh\left(\frac{d-x_p}{L_n}\right) + \cosh\left(\frac{d-x_p}{L_n}\right)} + \alpha_p L_n\right] \quad (25)$$

where $\gamma_n = \frac{S_n L_n}{D_n}$ and $\gamma_p = \frac{S_p L_p}{D_p}$

*Table 1. Parameters used in the computation.*

| Parameters | Values |
|---|---|
| $N_A$ | $3.6\times10^{22}$ m$^{-3}$ |
| $N_D$ | $3\times10^{24}$ m$^{-3}$ |
| $N_t$ | $10^{21}$ m$^{-3}$ |
| σ | $10^{-20}$ m$^{-2}$ |
| $\varepsilon_r$(InSb) | 17.7 [16] |
| $m_n^*$ (InSb) | $0.014m_0$ [16] |
| $m_p^*$ (InSb) | $0.43m_0$ [16] |
| $m_s$ (InSb) | $0.16m_0$ [17] |
| $m_{hh}$(InSb) | $0.40m_0$ [17] |
| Δ(InSb) | 0.81 eV [17] |
| $\varepsilon_r$ ($InAs_{1-x}Sb_x$) | 15.15+1.65x [18] |
| $m_n^*$ ($InAs_{1-x}Sb_x$) | $(0.023-0.039x+0.03x^2)m_0$ [18] |
| $m_p^*$ ($InAs_{1-x}Sb_x$) | $(0.41+0.02x)m_0$ [18] |
| $m_s$ ( $InAs_{1-x}Sb_x$) | $(0.14-0.04x)m_0$ [18] |
| $m_{hh}$($InAs_{1-x}Sb_x$) | $(0.4-0.18x+0.18x^2)m_0$ [18] |
| Δ ($InAs_{1-x}Sb_x$) | 0.39+0.42x [18] |
| $D_n$($InAs_{1-x}Sb_x$) | 0.1 m$^2$/s [18] |
| $D_p$($InAs_{1-x}Sb_x$) | 0.3 m$^2$/s [18] |

The net quantum efficiency can be written as

$$\eta(\lambda) = \eta_n(\lambda) + \eta_p(\lambda) + \eta_{dep}(\lambda) \tag{26}$$

The responsivity of the photodiode is the ratio of the photocurrent ($I_{photo}$) to the incident radiation power ($P_{op}$), given by

$$R = \frac{I_{photo}}{P_{op}} \tag{27}$$

## 3. Results and discussion

Numerical calculations have been performed for an $P^+$-InSb/π-$InAs_{1-x}Sb_x/N^+$-InSb long wavelength infrared region operating at 77 K. The incident photons with energy lower than bandgap of InSb cross the $N^+$ region with negligible absorption and get absorbed mostly in the narrow bandgap $InAs_{0.15}Sb_{0.85}$ region creating electron-hole pairs. Various parameters used in computation are listed in Table 1.

Fig. 3 shows the variation of the dark current density with the applied bias voltage at 77 K. The components constituting the dark density current e.g. diffusion, generation-recombination and tunneling (trap-assisted and band-to-band components) and their variations with the applied voltage are also shown in the figure. It is seen that the current density is mainly decided by the diffusion and generation-recombination components when the detector is forward biased. In the low reverse direction both band-to-band tunneling component and trap-assisted tunneling component of current density are found to play an important role in deciding the total reverse saturation current. However, the band-to-band tunneling component becomes very high as compared to the trap-assisted counterpart when the applied reverse voltage is high. Fig. 4 shows the variation of quantum efficiency of the photodetector with operating wavelength at 77 K and 300 K. The quantum efficiency of the photodetector has been estimated to be 48.7% at 5.4μm for operation 300 K and 43.0% at 3.8 μm for operation at 77 K. Fig. 5 depicts the variation of the voltage responsivity of the detector with wavelength for two different values of temperature (77 K and 300 K) as obtained theoretically on the basis of our model (solid line) and as reported experimentally (squares) by others [3]. The estimated variation of the voltage responsivity with wavelength is in fairly good agreement with the experimentally measured data in the long wavelength infrared region. There is however, a small discrepancy between theoretical results and experimental data in the shorter wavelength region at both the operating temperature. A compositional variation or gradient in the composition of material and for active region in the experimental work might be partially responsible for the reduction of the experimentally measured voltage responsivity in the shorter wavelength region. Absorption of incident radiation close to the GaAs/$N^+$-InSb interface region may also be responsible for the degradation of quantum efficiency at the shorter wavelength. The present model can not account for this absorption.

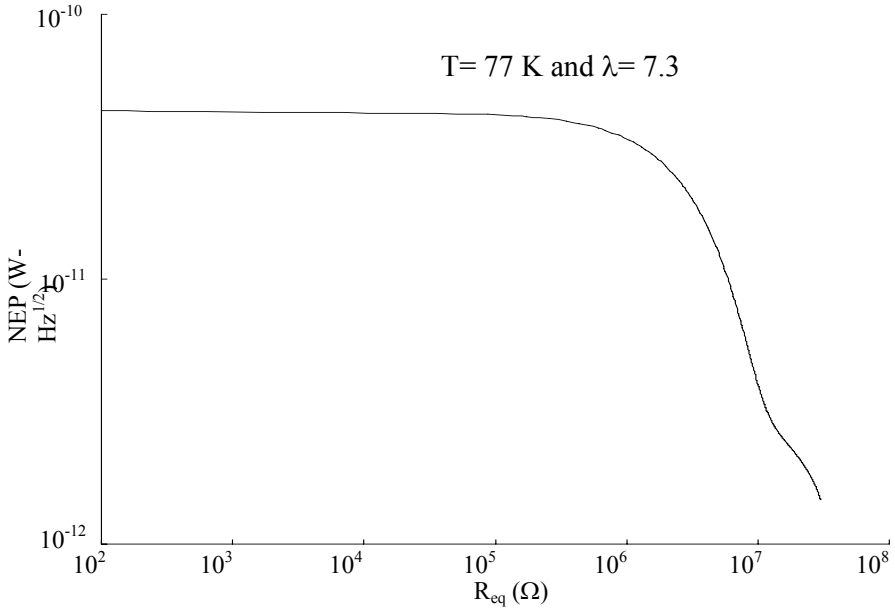


*Fig. 6. Variation of noise equivalent power (NEP) at 77 K with load resistance $R_{eq}$ for $\lambda$= 7.3 μm.*

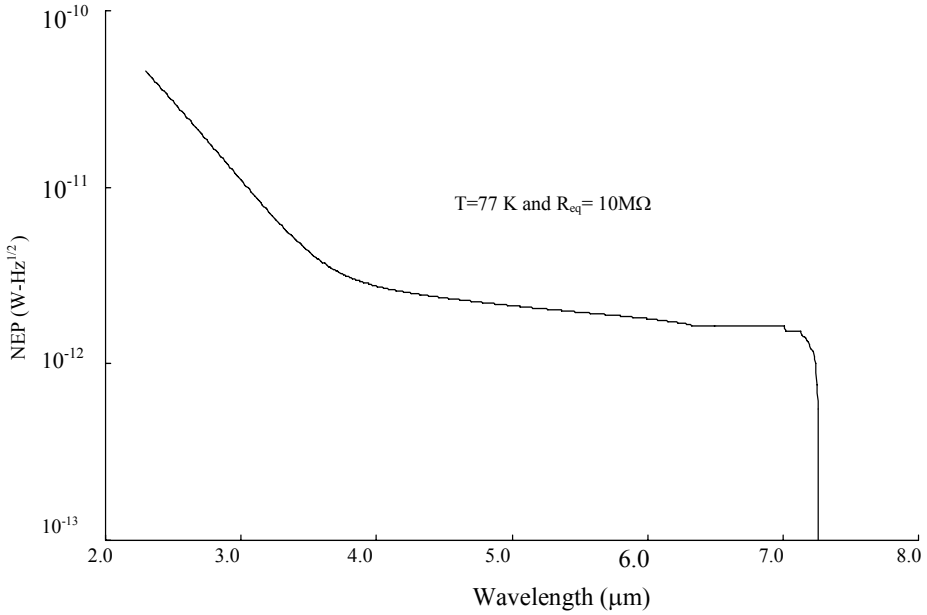


*Fig. 7. Variation of noise equivalent power (NEP) with wavelength of operation at 77 K for $R_{eq}$= 10 MΩ.*

An important figure of merit of the proposed photodetector for application in long-wavelength free space optical communication system is the noise equivalent power (NEP). The noise equivalent power of the detector depends on the equivalent load resistance which includes the diode resistance, bias resistance and the input resistance of the following amplifier. The variation of the theoretically estimated noise equivalent power (NEP) of the detector against the equivalent resistance of the photodetector for operation at 77 K is shown in Fig. 6. It is seen that so long as the equivalent resistance seen by photodetector is less than 1MΩ, the noise equivalent power of the photodetector is quite high (> $5\times 10^{-11}$ W Hz$^{-1/2}$) and therefore the receiver may not be very sensitive. However, the photodetector exhibits an extremely low noise equivalent power when the equivalent value of the resistor is 10 MΩ and the photodetector can be used to design a sensitive receiver. The photodetector can be used in conjunction with pre-amplifier designed to work in the high impedance (HZ) and transimpedance (TZ) mode to for develop of highly sensitive receiver. The variation of the noise equivalent power of the photodetector with operating wavelength is shown in Fig. 7 for operation at 77 K for an equivalent resistance of 10 MΩ. The photodetector exhibits a reasonably low noise equivalent power in operating wavelength region of 4-7 μm.

## 4. Conclusions

In this paper we presented a simplistic noise model of a long wavelength infrared (LWIR) photodetector taking into account of shot noise and thermal noise. The model can be used for theoretical characterization of electrical and optical properties of the detector for proposed application in free space optical communication systems at room temperature. The physics based model developed by us for simulation of photoresponse has been validated by reported experimental results. The present study reveals that the photodetector exhibits an extremely low noise equivalent power under suitable operating condition. It is suggested that the photodetector can be used with preamplifier operating in high impedance (HZ) and transimpedance (TZ) configuration to develop a highly sensitive optical receiver for free space optical communication applications. The model can be used as a tool by the design engineers for optimization of the detector for the best performance in respect of noise equivalent power and responsitivity.

**Acknowledgement**

The authors wish to acknowledge the Council of Scientific and Industrial Research (CSIR), Govt. of India for the financial support (Grant No.:22(0400)/06/EMR-II).

## References

[1] H. Manor, S. Arnon, Applied Optics **42**, 4285 (2003).
[2] N. S. Kopeika, J. Bordogna, Proc. IEEE, **58**, 1571 (1970).

[3] J. D. Kim, D. Wu, J. Wojkowski, J. Xu, J. Piotrowski, E.Bigan, M. Razeghi, Appl. Phys. Lett. **67**, 2645 (1995).
[4] A. Rogalski, Prog. Quant. Electr. **15**, 191 (1989).
[5] J. D. Kim, M. Razeghi, Opto-Electr. Rev. **6**, 191 (1989).
[6] A. Krier, H. H. Gao, Y. Mao, Semicond. Sci. Technol. **13,** 950 (1998).
[7] J. Piotrowski, W. Gawron, Infrered Phys. Technol. **36,** 1045 (1995).
[8] J. Piotrowski, W. Galus, M. Grudzien, Appl. Phys. Lett. **31**, 1 (1991).
[9] Y. Tian, B. Zhang, B. Jiang, Y. Jin, IEEE Trans. Electron. Devices **47**, 544 (2000).
[10] A. Rogalski, R. Ciupa, W. Larkowaski, Solid-state Electron., **39**, 1593 (1996).
[11] T. N. Cassalman, P. E. Peterson, Solid State Commun. **33**, 615 (1980).
[12] A. Roglaski, Z. Orman, Infrared Phys. **25**, 551 (1985).
[13] B. L. Gelmont, Phys. Lett. **66A**, 323 (1978).
[14] A. Rogalski, K. Adamiec, J. Rutkowski, SPIE Press Bellingham, Washington, USA, 2000.
[15] V. Gopal, S. Gupta, P.K. Bhan, R. Pal, P. K. Chaudhary, V. Kumar, Infrared Phys. Technol. **43**, 143 (2003).
[16] S. M. Sze, Willy Eastern Ltd., New Delhi, 1981.
[17] M. Levinshtein, S. Rumyantsev, M. Shur, "Handbook series on Semiconductor parameters," vol.1, World Scientific, London, 1999.
[18] M. Levinshtein, S. Rumyantsev, M. Shur, "Handbook series on Semiconductor parameters," vol. 2, World Scientific, London, 1999.

*Corresponding author: pchakra@bhu.ac.in